Cell Reports
Physical Science

CellPress
OPEN ACCESS

Article

Topologically non-trivial metal-organic assemblies inhibit β_2-microglobulin amyloidogenesis

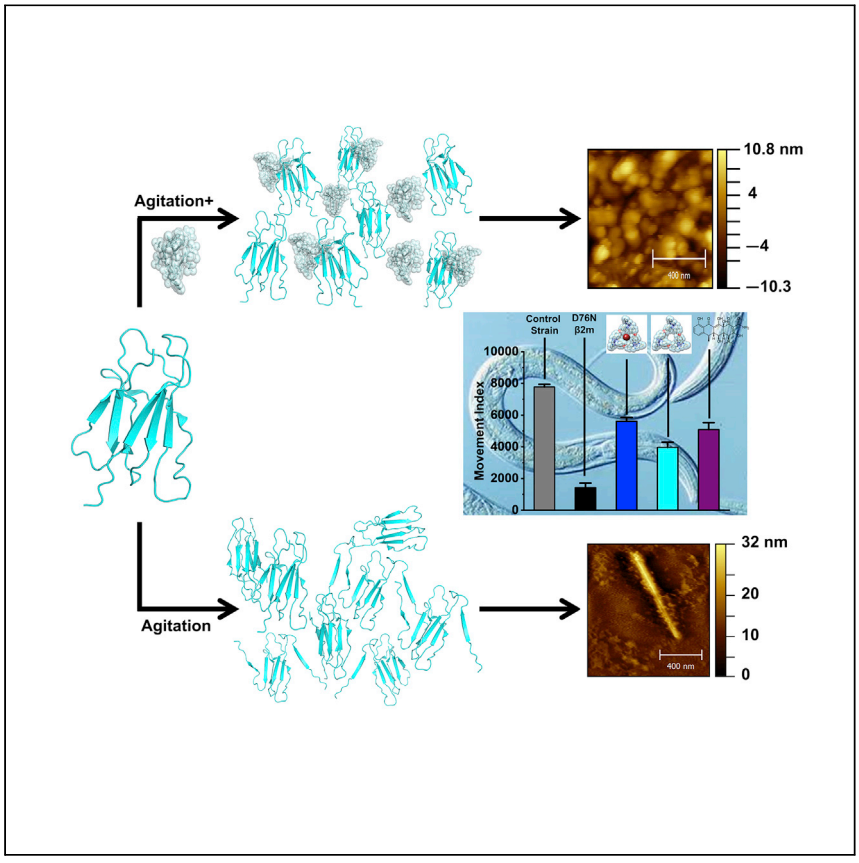

Prakasam et al. report that topologically non-trivial metal-organic species inhibit the *in vitro* fibrillogenesis of the paradigmatic amyloidogen β_2-microglobulin and the effects of the D76N mutant expression in a *Caenorhabditis elegans* disease model. Acting as small-molecule chaperones, the metal-templated assemblies suppress the formation of soluble protofibrillar oligomers by engaging labile supramolecular interactions that interfere with protein-protein pairing.

Thirumurugan Prakasam, Yamanappa Hunashal, Cristina Cantarutti, ..., John-Carl Olsen, Ali Trabolsi, Gennaro Esposito

ali.trabolsi@nyu.edu (A.T.)
rino.esposito@nyu.edu (G.E.)

Highlights

Topologically non-trivial (TnT) species may engage labile supramolecular interactions

Proteins can be ideal targets of TnT metal-templated structures

Protein fibrillogenesis can be inhibited by TnT metal-organic assemblies

Rigidity and dimensions of the TnT assemblies modulate interactions with proteins

Prakasam et al., Cell Reports Physical Science 2, 100477
July 21, 2021
https://doi.org/10.1016/j.xcrp.2021.100477

Cell Reports
Physical Science

CellPress
OPEN ACCESS

Article

Topologically non-trivial metal-organic assemblies inhibit β_2-microglobulin amyloidogenesis

Thirumurugan Prakasam,[1] Yamanappa Hunashal,[1,2] Cristina Cantarutti,[2] Sofia Giorgetti,[3] Giulia Faravelli,[3] Valentina Mondani,[3] Sudhir Kumar Sharma,[4] Ramesh Jagannathan,[4] Giovanni Palmisano,[5] Vittorio Bellotti,[3,6] Federico Fogolari,[7,8] John-Carl Olsen,[9] Ali Trabolsi,[1,*] and Gennaro Esposito[1,8,10,*]

SUMMARY

Inhibiting amyloid aggregation through high-turnover dynamic interactions could be an efficient strategy that is already used by small heat-shock proteins in different biological contexts. We report the interactions of three topologically non-trivial, zinc-templated metal-organic assemblies, a [2]catenane, a trefoil knot (TK), and Borromean rings, with two β_2-microglobulin (β2m) variants responsible for amyloidotic pathologies. Fast exchange and similar patterns of preferred contact surface are observed by NMR, consistent with molecular dynamics simulations. *In vitro* fibrillation is inhibited by each complex, whereas the zinc-free TK induces protein aggregation and does not inhibit fibrillogenesis. The metal coordination imposes structural rigidity that determines the contact area on the β2m surface depending on the complex dimensions, ensuring *in vitro* prevention of fibrillogenesis. Administration of TK, the best protein-contacting species, to a disease-model organism, namely a *Caenorhabditis elegans* mutant expressing the D76N β2m variant, confirms the bioactivity potential of the knot topology and suggests new developments.

INTRODUCTION

Under conditions of compromised homeostasis, proteins misfold and exhibit a general propensity to aggregate into self-assembled fibrils that are characterized by cross-β structure—in other words, a supramolecular arrangement of paired β strands known as amyloid.[1,2] Amyloid deposits in organs and tissues are associated with neurodegenerative diseases (e.g., Alzheimer's disease, Parkinson's disease), specific functional degenerations (e.g., cataracts, carpal tunnel), and systemic pathologies (e.g., type 2 diabetes, amyloid light-chain [AL] amyloidosis).[3] One strategy for preventing amyloid formation is to administer drugs that bind and stabilize aggregation-prone proteins,[4,5] as does the benzoxazole tafamidis with tetrameric transthyretin (TTR),[6] some antibodies with Aβ peptide oligomers,[7–9] or antibody fragments (nanobodies) with lysozyme[10] or β_2-microglobulin (β2m)[11] variants. Nevertheless, tight binding to fibrillogenic or protofibrillar proteins to counter the pathologic effects of amyloid aggregation is not necessarily the easiest nor the most convenient approach to pursue. Even for the mentioned benzoxazole, which has already been approved for treatment of TTR amyloidosis, an alternative mechanism of the onset of pathology[12] raises questions about the efficacy of the

[1]Science Division, New York University at Abu Dhabi, Abu Dhabi, UAE

[2]DAME, Università di Udine, 33100 Udine, Italy

[3]Dipartimento di Medicina Molecolare, Università di Pavia, 27100 Pavia, Italy

[4]Engineering Division, New York University at Abu Dhabi, Abu Dhabi, UAE

[5]Chemical Engineering Department, Khalifa University, Abu Dhabi, UAE

[6]Wolfson Drug Discovery Unit, Centre for Amyloidosis and Acute Phase Proteins, Division of Medicine, University College London, London NW3 2PF, United Kingdom

[7]DMIF, Università di Udine, 33100 Udine, Italy

[8]INBB, 00136 Roma, Italy

[9]Department of Chemistry, RC Box 270216, University of Rochester, Rochester, NY 14627, USA

[10]Lead contact

*Correspondence: ali.trabolsi@nyu.edu (A.T.), rino.esposito@nyu.edu (G.E.)

https://doi.org/10.1016/j.xcrp.2021.100477

complexation strategy. In fact, a proposed class of anti-amyloid drugs, typically small molecules, establish, with their protein counterparts, non-specific and more or less dynamic interactions based essentially on transient hydrophobic and hydrophilic interactions such as π-stacking and hydrogen bond formation,[4,5] i.e., the same type of supramolecular interactions that drive amyloid assembly.[2] This dynamic contact mode is very much reminiscent of the action of the small heat shock proteins (sHsps), also referred to as small heat shock molecular chaperones, that interact with and stabilize long-lived intermediate states of proteins on their off-folding pathway, before aggregation.[13] No refolding is achieved, but aggregation and precipitation are avoided by fast formation and disruption of labile adducts. For example, the dynamic interaction of a sHsp such as αB-crystallin has been shown to prevent the amyloid formation of Aβ peptide, β2m, apolipoprotein C II, α-synuclein, and κ-casein.[14,15] Hence, small molecules whose fast-exchange interactions are capable of interfering with fibrillogenesis can be viewed as small-molecule chaperones[16,17] or pharmacological chaperones acting against protein homeostasis dysfunction and misfolding diseases, as recently reviewed.[18,19] Along this line, the tetracyclines have been shown to inhibit the aggregation of amyloidogenic proteins *in vitro* and to ameliorate the symptoms of some amyloid-associated diseases.[17,20,21] In addition to small organic molecules, nanoparticles (NPs) have also displayed fast-exchange interactions with amyloidogenic proteins that successfully interfere with fibrillogenesis *in vitro*,[22–24] although the conditions and the characteristics of some protein-NP systems may also increase the rate and extent of the fibrillar aggregation.[25] Attempts to modulate or reproduce protein interactions have also been carried out using synthetic species exhibiting non-trivial 3D geometry provided by cystine-rich cyclic peptides called cyclotides,[26,27] or short peptides with multiple cystine-knots called knottins.[28,29] Thanks to their chemical nature, these compounds may advantageously exploit the same chemical characteristics of the proteins to perform their function, in many cases without undergoing rapid proteolysis in a cellular environment.

Here, we describe the interactions, between each of three synthetic, topologically non-trivial metal-organic structures, a [2]catenane ([2]C), a trefoil knot (TK), and Borromean rings (BR), and amyloidogenic proteins. The three structures effectively inhibit fibrillogenesis *in vitro* and, in the case of TK, nearly remove the pathologic effects *in vivo*. The metal-templated structures were synthesized as acetate (Ac) or trifluoroacetate (TFA) salts from a pair of organic ligands—2,6-diformylpyridine and ((([2,2′-bipyridine]-4,4′-diylbis(methylene))bis(oxy))bis(4,1-phenylene))dimethanamine—and the corresponding Zn salts (Figures 1A and S1), to obtain, respectively, the Zn^{2+} complexes [2]C●4Ac, TK●6TFA, and BR●12TFA, as previously described.[30–32] In addition, the TK can accommodate two bromide anions in its central cavity, a modification that enhances the rigidity of the complex.[30,31] For this reason, we also tested the TK in which two TFA counterions were exchanged for two centrally lodged bromide anions. We refer to this complex as TK-Br, and to the TK●6TFA complex as TK-TFA. For the Zn-templated complexes of [2]catenane and Borromean rings, we use the shorthand notations [2]C and BR, respectively. The metal-free TK (TK-ΔZn), which is more flexible than the metal-containing TK was also studied. The idea of exploring the interactions of all of these species with amyloidogenic proteins was suggested by the consideration that those supramolecular interactions that are typical of the proteins' repertoire and are heavily involved in amyloid fibril assembly[2] could also be established by the metal-organic structures formed by the above-mentioned chemicals, whose non-trivial topology had repeatedly been shown.[30–32]

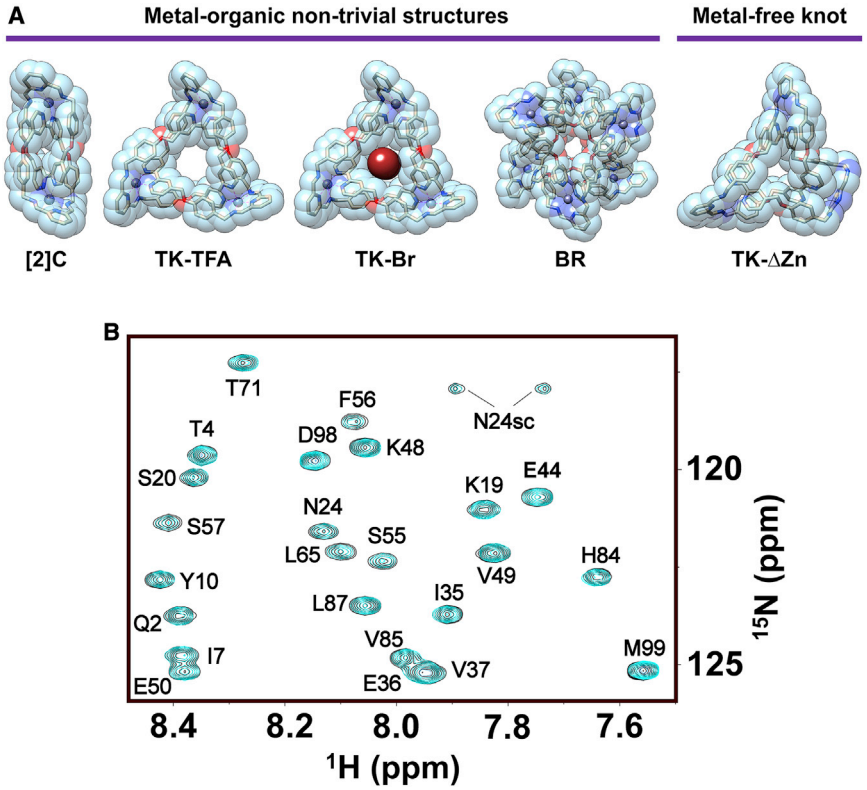

Figure 1. Structures of the considered non-trivial metal organic complexes and their effect on the NMR spectrum of β2m

(A) Illustrations of the single-crystal X-ray structures of the topologically non-trivial metal-organic species $[2]C^{4+}$, TK^{6+}, $(TK\bullet 2Br)^{4+}$, BR^{12+}, and the modeled structure of the metal-free TK-ΔZn, whose protein interactions were studied. The metal-containing species are shown here devoid of their respective counterions, except for $(TK\bullet 2Br)^{4+}$, in which 2 bromide ions (red spheres) sit in the central cavity[30,31] and partially replace the trifluoroacetate (TFA) neutralization of TK^{6+} (TK-TFA). TK-ΔZn is obtained from imine bonds reduction and metal removal (see the Materials subsection in Experimental procedures) and exhibits the same knotted topology as is present in the metal-containing knot. The chemical structure formulae of all of the species are given in Figure S1.

(B) Region from the overlay of ^{15}N-^{1}H HSQC spectra of 59 μM β2m without (black contours) and with (cyan contours) 69 μM TK-TFA. SC indicates side chain NH connectivities. The entire 2D map is shown in Figure S2B.

The amyloidogenic proteins studied were β2m and its naturally occurring mutant D76N β2m. Wild-type β2m is an 11.9-kDa protein that functions normally as the non-polymorphic component of the major histocompatibility complex but precipitates and thus causes a tissue-specific amyloidosis in patients undergoing long-term dialysis.[33] The variant protein D76N β2m—which bears a mutation at residue 76, with an asparagine in place of aspartate—is responsible for an aggressive hereditary systemic amyloidosis.[34,35] Interactions between the metal-organic species and the proteins were studied by NMR spectroscopy, fluorescence, atomic force microscopy (AFM), and molecular dynamics (MD) computations. We found that, in solution, all of the metal-templated structures establish dynamic and preferential contact at approximately the same locations of the surfaces of the proteins and that they prevent fibrillar aggregation of D76N β2m. The TK complexes exhibited a more efficient interaction pattern than [2]C and BR, likely due to possessing optimal size, shape, rigidity, and solvation characteristics relative to the target proteins. The more flexible and hydrophobic TK-ΔZn also made significant contact with the

proteins, but induced aggregation and did not inhibit fibril formation *in vitro*. Administration of TK complexes to a transgenic *Caenorhabditis elegans* strain expressing D76N β2m sharply reduced the expression-related impairment and confirmed also *in vivo* the efficacy of the Zn-templated species with better interaction performance. Overall, these results represent a proof-of-concept for a possible avenue to interfere with protein-protein interactions. To contrast amyloid aggregation with the same type of supramolecular interactions that determine the onset of the process, it is possible to resort to topologically non-trivial compounds with suitable dimension and rigidity. The chemical properties of these compounds that are essential to establish the competing supramolecular interactions may be tuned in principle to enforce high affinity for the target proteins while preserving kinetic lability of the ensuing adducts.

RESULTS

β2m structure is preserved upon weak but specific interaction with TKs

To initiate this study, we monitored the interactions between the metal-organic knots (TK-TFA and the more stable TK-Br[30,31]) and the wild-type β2m by one-dimensional (1D) ^{1}H NMR. Direct inspection of the largely dispersed aromatic region of the TK spectra[30,32] was, however, hampered by the overlapping signals from the protein (Figure S2A). The protein used in NMR experiments was ^{15}N-uniformly labeled, which allowed 2D ^{15}N-^{1}H heteronuclear single quantum coherence (HSQC)[36] spectra to be collected during the titrations (Figures 1B and S2B).

In the presence of TK-TFA, the chemical shifts of the protein's backbone and side chain NHs were essentially the same as those observed for the protein alone, as the largest variations ($\Delta\delta$) observed for a few signals—typically the side chain amides corresponding to N21, N24, and Q89 and the backbone amides corresponding to H13, F22, G29, and R97—were comparable to the experimental resolution uncertainty of the combined ^{15}N-^{1}H chemical shifts ($\pm 9.8 \times 10^{-3}$ ppm)[37] and therefore meaningful with respect to average $\Delta\delta$ values of $(2.8 \pm 2.0) \times 10^{-3}$ ppm (Figure S3). The most significant net effect of the TK-TFA concentration increase on β2m HSQC spectra was an overall progressive decrease in the cross-peak intensities. This decrease, however, proved to be unevenly distributed over the whole protein spectrum (Figure S4A). An analogous pattern of peak attenuation was observed when the more rigid TK-Br[30,31] was assayed (Figure S4B). However, at equimolar protein:TK-Br concentrations, the average signal attenuation of the HSQC spectrum of the protein was 12% larger than with TK-TFA. In addition, especially when KBr (2.8 mM) or NaCl (100 mM) were present in solution, larger $\Delta\delta$ values (2- to 3-fold the experimental uncertainty) were measured for the few locations previously mentioned and for S11, R12, E16, H51, F56, S61, and N83 (Figure S3A and S3B), with the remaining signals conserving about the same chemical shift as the isolated protein. It should be noted that the meaningful $\Delta\delta$s and their increases with ionic strength occurred most frequently at amides coinciding with or adjacent to Asn, Gln, Asp, Glu, Ser, and Thr residues. This suggests that the interaction with TK-Br and TK-TFA affects the H-bonding and/or solvation pattern of side chain carboxylates, carboxy-amides, and hydroxyls of the protein, besides sampling unevenly several other accessible locations of the protein, as inferred from the attenuation of the corresponding NMR signals. Significantly, an ionic strength level comparable to the physiological one affected only the interactions involving hydrophilic sites on the protein surface, but did not induce any precipitation or instability in the equimolar β2m-TK-Br mixture. Also, the signal attenuation pattern appeared substantially unaffected by the ionic strength. Since the invariance of the translational diffusion coefficients measured by diffusion ordered spectroscopy (DOSY)[38] rules out the induction

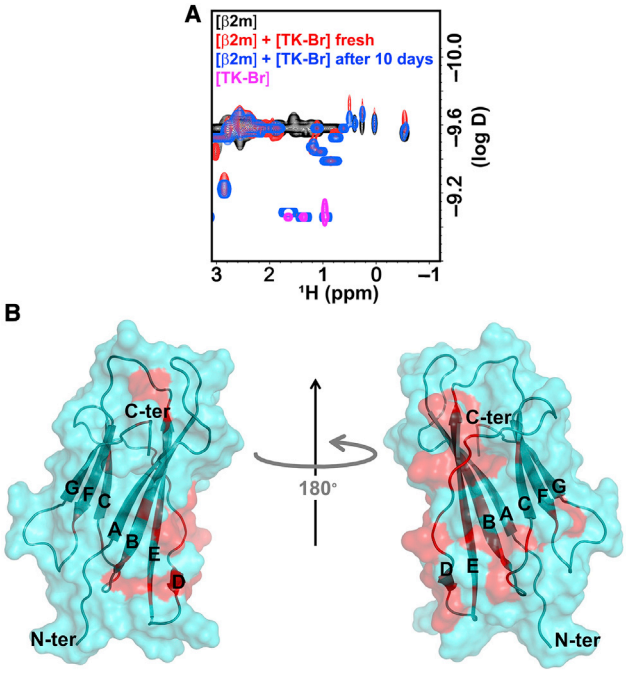

Figure 2. Diffusion coefficient and interaction surface of β2m in the presence of TK

(A) Overlay of the aliphatic region of DOSY spectra obtained from 82 μM β2m solutions (black contours), 82 μM β2m solutions with 94 μM TK-Br, either freshly prepared (red contours) or 10 days after preparation (blue contours), and 108 μM aqueous TK-Br (purple contours). The deviations of the DOSY for the samples with TK-Br are an artifact due to the overlap of protein and TK-Br signals. Where no such overlap occurs, the diffusion coefficient of the protein does not change in the presence of TK-Br.

(B) Illustration of β2m showing, with red highlights, the locations of the amino acid residues that give rise to the most attenuated HSQC NH peaks—at least one standard deviation (SD) with respect to the average attenuation (Figure S4)—as a consequence of the fast-exchange interaction with TK-TFA. The involved regions are primarily strand D, loop DE, and part of strand E, as well as the other adjacent and accessible locations on the same sheet (i.e., strand B and loop CD), and on the opposite sheet (i.e., the contiguous edges of strands C, F, and loop BC), and the C-terminal segment. With TK-Br, strand A and loop EF of the former sheet are also involved. The reproduced structure is the NMR solution structure of β2m (PDB: 1JNJ).[39] The secondary structure elements of β2m are indicated according to the crystallographic naming scheme (PDB: 3HLA).[40] Structures are drawn with PyMOL (Schrödinger Inc.).

of appreciable changes in β2m association equilibria[15] by the TKs (Figure 2A), we conclude that the attenuation of the protein HSQC NH peaks reflects line broadenings due to chemical exchange and possibly transient dipolar contributions originating from the dynamic interaction with the TK species. The same interaction regime is also reported by the limited chemical shift changes of a few specific signals of the protein. Thus, as inferred from the substantial invariance of the HSQC chemical shifts in the presence of TK-TFA or TK-Br, the β2m structure is conserved. However, a preferentially oriented, fast exchange interaction does occur, as indicated by the uneven pattern in the decrease in the intensities of the amide signals of the protein and by the small but meaningful Δδ values of certain amide signals. As reported in Figure 2B, the preferential interaction involves, with either TKs, approximately the same protein regions.

Interactions between the β2m motif and other Zn-templated non-trivial structures

The encouraging results obtained with TK complexes and wild-type β2m prompted us to study the interactions that other topologically non-trivial metal-organic

structures of different size and shape would have with the protein. In these experiments, we switched to the mutant D76N β2m and systematically investigated its interactions with the Zn-templated complexes [2]C, TK-Br, and BR. In spite of the structural invariance associated with the mutation,[34] the thermodynamic stability of D76N β2m is significantly decreased (by ~50%) under physiological conditions, and simultaneously the fibrillogenic tendency is greatly enhanced, with respect to the parent species,[34,35] which made the D76N variant ideal for distinguishing the effects of the three Zn-templated structures. The interactions of D76N β2m with TK-Br and the smaller ([2]C) or larger (BR) dimension analogs were mapped by NMR using the same approach as used with the wild-type protein. The observed effects in ^{15}N-^{1}H HSQC spectra recapitulate the fast exchange pattern, with uneven attenuation of the cross-peak intensities and substantial lack of chemical shift changes, except for those deviations detected also with the wild-type protein and involving carboxylate, carboxy-amide, and hydroxyl-containing residues at the edges of the AB loop and the facing C-terminal segment, and, on the opposite extremity of the molecule, at the FG loop ends and the neighboring BC loop. This distribution pattern was reproduced with all of the Zn-templated species, with average $\Delta\delta$ values decreasing in the order TK-Br > [2]C > BR. It is worth mentioning that, with D76N β2m and the three considered metal-organic species, we deal with average $\Delta\delta$ values that are at most comparable with the experimental resolution limit (9.8×10^{-3} ppm), namely $(1.0 \pm 1.1) \times 10^{-2}$, $(7.6 \pm 8.6) \times 10^{-3}$, and $(4.5 \pm 3.1) \times 10^{-3}$ ppm in the presence of TK-Br, [2]C, and BR, respectively. We rely, however, on chemical shift deviations that are typically 2–3 times that resolution limit, in practice the same as observed with wild-type β2m in the presence of salts. This highlights a somewhat larger "sensitivity" of the D76N variant compared with the wild-type isoform to the tested compound class. The NMR results confirm that the structure of D76N β2m was consistently preserved in solution in the presence of the metal complexes. The extent of signal attenuation in the protein HSQC spectra, however, was dependent on the interacting species. The average relative intensities and corresponding standard deviations ($RI_{av} \pm SD$), measured from the ratios of the cross-peak intensities in the presence and absence of [2]C, TK-Br, or BR, were 0.72 ± 0.09, 0.59 ± 0.12, and 0.89 ± 0.07, respectively (Figures S5 and S6). These RI_{av} values of the NH signals indicate that the protein spectrum perturbation, reflecting contact area and transient adduct lifetime, increases on moving from [2]C to TK-Br, but sharply decreases with BR. The amount of attenuation measured for the variant D76N with TK-Br was also larger than the corresponding effect observed for wild-type protein with TK complexes (Figure 2B), primarily because of an affinity gain due to the decreased charge of the mutant. This seems a clear indication of hydrophobic interaction predominance. The same should apply to all of the examined metal-organic partners of D76N β2m, as supported by comparing the effect of BR on wild-type and mutant proteins, in the presence of 100 mM NaCl (Figures S7 and S8). Only slight variations of the average $\Delta\delta$s and intensity attenuations were measured for D76N β2m with any of the addressed complexes in the presence of 100 mM NaCl with or without buffer (5 mM $NaHCO_3$) (Figures S9A and S9B). Although variable in intensity, D76N β2m interactions with the three different Zn-templated structures appeared structurally equivalent as was observed for the wild-type protein with the different TK complexes and BR. Therefore, the presence of different counterions balancing the Zn^{2+} charges, namely Ac for [2]C, TFA and Br^- for TK-Br, and TFA for BR, does not affect significantly the interaction pattern. This can be readily appreciated from the illustrations of Figure 3 in which the red color highlights the protein regions whose signal were most attenuated by the presence of the three metal-organic complexes (see also Figures S10A and S10B). Relevant details are reported in the legend of Figure 3. The

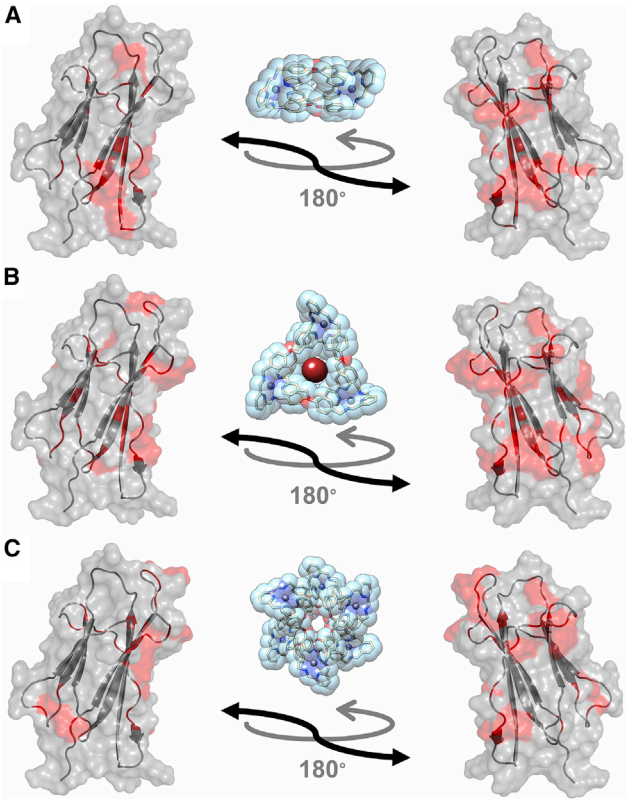

Figure 3. Interaction of D76N β2m with different Zn-templated structures

Sites of interaction between D76N β2m and [2]C (A), TK-Br (B), and BR (C) are highlighted in red in the illustrations of the protein. Sites of interaction were inferred from the relative intensity (RI) values of the HSQC amide peaks determined for 50 or 100 μM protein solutions, in the absence and equimolar presence of the indicated Zn-templated complex. Given the broad extent of the observed effects on the NMR spectrum of D76N β2m (Figure S5) compared to those apparent in the spectrum of the wild-type protein (Figure 2B), the red highlighting depicts RI $\leq$ (RI_{av} − SD/2) for any species to stress properly the sizeable attenuations induced by [2]C and TK-Br and the corresponding similarities with the weakly attenuating BR. From these depictions, a largely coincident interaction surface becomes apparent. The surface is composed, on one sheet, of residues of strand D, residues near the beginning of strand E, strand B, and residues near the end of the CD loop; and, on the opposite sheet, of the contiguous edges of strand C, strand F and loop BC, and the C-terminal segment. Additional involvement of the segments of loop AB adjacent to the end of strand A and the beginning of strand B is observed with TK-Br and BR, whereas with [2]C, the interaction at strands D and E extends to the intervening loop DE. Labeling of the elements of the structures is consistent with the crystallographic annotations for wild-type β2m (PDB: 3HLA).[40] The NMR solution structure of the latter (PDB: 1JNJ)[39] is used for any D76N β2m drawings, given the conformational analogy of both variants.[34,35]

lability of the interactions that were mapped by NMR was confirmed also by microcalorimetric measurements conducted under similar conditions (data not shown). No thermodynamic parameter could be estimated to reveal an appreciable binding.

MD simulations

Different species were submitted to MD simulations. In particular, to retrace the experimental NMR examination, the interactions of wild-type β2m were considered only with TK-Br, whereas the interactions of the D76N variant were simulated with all of the metal-templated structures. The contacts between the wild-type protein and TK-Br, are pictorially presented in Figure 4A. The adjacent panel (Figure 4B) displays

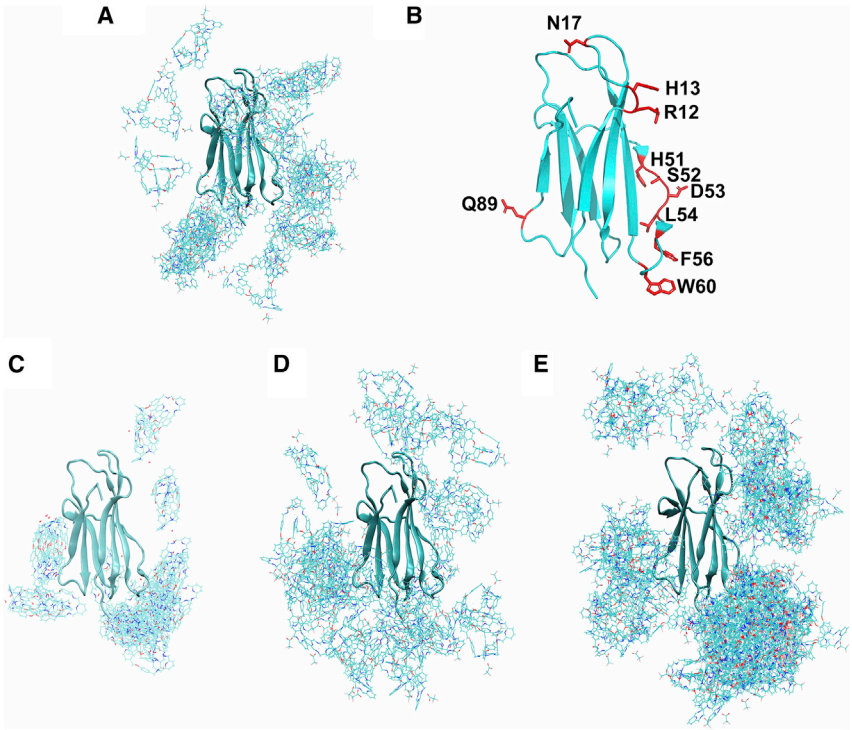

Figure 4. Interaction modeling by molecular dynamics (MD)

MD snapshots showing protein contacts with the considered metal-organic species. The snapshots sampled over 10 ns MD are overlaid.

(A) Contacts of wild-type β2m and TK-Br.

(B) Most frequently contacting residues explicitly indicated and shown in sticks in the illustration of β2m.

(C–E) Contacts of D76N β2m and [2]C (C), TK-Br (D), and BR (E).

the residues of the protein that are mostly involved in those interactions. Simulations show that contacts are formed and broken dynamically and that no complexes of long-term stability are formed. The protein regions establishing the largest number of contacts on average with TK-Br are, in order of importance, the DE loop with the aromatic residue W60; the D strand with residues H51, S52, D53, L54, and F56; loop AB with R12, H13, and N17; and loop FG with Q89 (Figures 4A and 4B). These positions are in good agreement with the NMR attenuation pattern, although it should be noted that HSQC spectra monitor only the resolved NH signals, whereas the MD short-range contacts are computed for any backbone and side chain atom of the structure residues. For instance, some DE loop locations of β2m are in fact attenuated in the presence of TK-Br (Figure 2B), but no information can be obtained for W60 due to the exchange broadening impairing the observation of the corresponding backbone and side chain peaks.

The MD runs of D76N β2m with any of the considered Zn-templated structures always produced a variety of transient adducts and no stable complex formation, as obtained with TK-Br and wild-type β2m. The different sizes of [2]C, TK-Br, and BR affect the number of contacts and the lifetime of the adducts, with the largest structure, BR, establishing more and longer-lasting contacts. A comparison of the relative frequency of ligand-protein contacts in the three MD simulations of D76N β2m (Figures 4C–4E) confirms the occurrence of the most relevant contacts in loops DE, BC, FG, and AB and strands D and E, with all of the tested metal-organic structures, in

agreement with the NMR evidence (Figure 3). The same residues as illustrated in Figure 4B establish the most prominent contact fractions in D76N as well, although the distribution statistics vary for each metal-templated species. In addition, the simulations also highlight some interaction differences of the protein with the individual metal-organic assemblies, such as the increased involvement of loop BC and following strand C in [2]C and TK-Br contacts, nicely reproducing the experimental NMR results.

The Zn-templated complexes inhibit fibrillogenesis *in vitro*

Fibrillogenesis of D76N β2m was monitored by the thioflavin T (ThT) fluorescence assay and AFM, according to well-established protocols.[34,35] The necessity of conducting the experiments in the presence of the metal-organic complexes enforced the testing of only aqueous samples of D76N β2m. When agitated in buffer-free water (pH 6.6–6.8), i.e., under conditions that ensure the stability of the examined metal-organic species, D76N β2m fibrillates.[24,34,35] Wild-type β2m, on the other hand, requires quite acidic pH[41] to fibrillate *in vitro*. However, our Zn-based structures cannot be studied in acidic solution, which causes hydrolysis of their imine bonds (Figures S11A and S11B). Although the considered metal-organic complexes are stable in buffers such as phosphate (Figure S12), HEPES, or bisTris, and their solutions with wild-type or D76N β2m can be studied without problems in a physiologic-like buffered ambient solution ($NaHCO_3$ 5 mM, NaCl 100 mM, pH 7.2), we used unbuffered water because the actual isoelectric point (pI) of D76N variant is close to neutrality.[34,35] Thus, it is possible to rely on the buffering capacity of the protein itself to avoid possible partial quenching effects of ThT fluorescence arising from buffer and salt anions.[42] Figures 5A–5C report the time course of ThT fluorescence, as monitored on incubating, under fibrillogenic conditions, the D76N β2m variant alone or in presence of [2]C, TK (either TFA or Br) or BR, all at the same concentration as the protein, i.e., 20 μM. The typical ThT fluorescence enhancement arising from fibril formation was observed only in the samples that contained the protein alone, whereas no hint of fibril formation was detected when any of the considered Zn-templated species was present. Control fluorescence determinations carried out on the isolated metal-organic structures showed an emission maximum at 345 nm (Figure S13) and absorption maxima at 300 and 310 nm—wavelengths values quite distinct from ThT excitation and emission wavelengths (445/480 nm). The addition of TK-Br to preformed D76N β2m fibrils had no suppressing or reducing effect on the ThT fluorescence level that was reached under fibrillogenic conditions (Figure S14A). This indicates that the TK-Br does not affect preexisting fibrils. [2]C and BR were not tested in this assay, as it was inferred that they too would not dissolve or disrupt pre-formed fibrils, due to their weaker interactions with D76N β2m (Figures 3 and S5–S10). Images obtained by AFM of protein samples submitted to fibrillogenic treatment, in the presence or absence of the different metal-organic structures, are shown in Figures 5D–5G. The samples with [2]C, TK-Br, and BR (Figures 5E–5G) show approximately spherical NPs with diameters that typically range ~100 nm. In contrast, elongated fibrils are seen in the sample from the solution of the isolated protein (Figure 5D), which is consistent with the results of the ThT assay. The length of typical fibrils ranges from 0.5 to 1 μm.

Effect of the organic scaffold, TK-ΔZn

The inhibition of fibrillogenesis that was consistently observed when D76N β2m samples were incubated with the metal-templated structures is intriguing, especially considering the type of interaction occurring between the different species. The pattern illustrated by Figures 1, 2, and 3 is essentially consistent with a weak interaction that occurs through fast exchange, which seems counterintuitive in

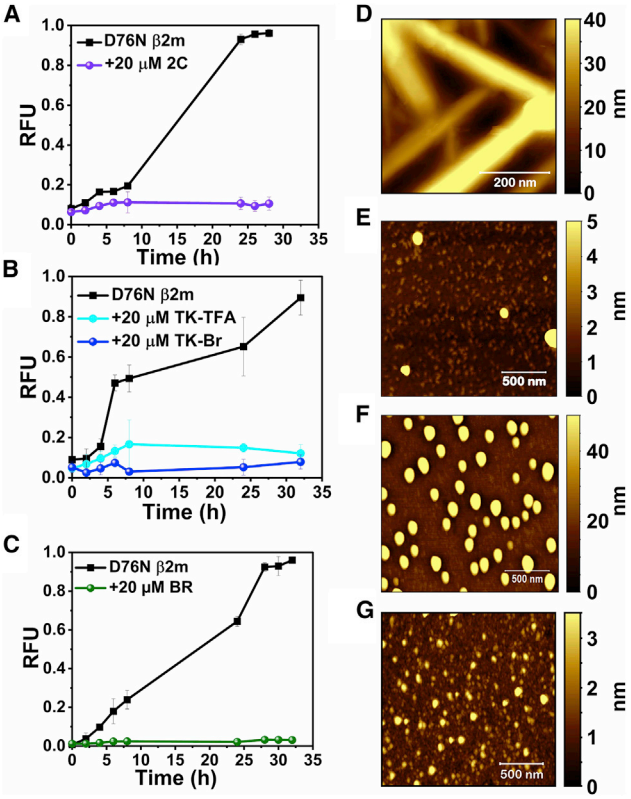

Figure 5. D76N β2m fibrillogenesis assessment

(A–C) Time course of ThT fluorescence (in relative fluorescence units, RFUs), measured for 20 μM D76N β2m solutions kept under fibrillogenic conditions at 37°C in the absence and presence of 20 μM [2]C (A), 20 μM TK-Br or TK-TFA (B), and 20 μM BR (C). The ThT concentration was 10 μM. The lines joining the experimental points are only guides for the eye. The reported error bars are the SDs of the 3 measurements that were performed for any experimental point. A more detailed ThT fluorescence control at higher time resolution, with the relative fitting of the raising phase, is reported in Figure 6D.

(D–G) AFM profiles obtained on samples from a 20-μM D76N β2m control solution (D) and from 20 μM D76N β2m + 20 μM [2]C (E), 20 μM D76N β2m + 20 μM TK-Br (F), and 20 μM D76N β2m +20 μM BR (G) mixtures, all kept under fibrillogenic conditions at 37°C for 36 h (same as used for ThT assays). For the sample in (D), the average fibril length and thickness were 650 ± 100 and 90 ± 30 nm, respectively. For the samples in (E)–(G), the average particle diameter was 99 ± 33 nm. Additional AFM images relative to protein/TK-TFA samples and control samples of TK-Br alone are shown in Figures S14B and S14C, respectively.

consideration of the final effect, which is the inhibition of a massive, ordered aggregation process. The efficient turnover of labile interactions is, however, also the signature of small-molecule chaperones such as doxycycline, a tetracycline that has been proven to prevent β2m fibrillogenesis *in vitro*[17] and that is being used successfully as a therapy to alleviate the impairment caused by β2m amyloid deposits.[20] To ascertain whether the inhibition of fibrillogenesis documented in Figures 5 and S14 could be attributed to a generic chemotropism of the organic scaffolds of the tested metal-organic complexes for the β2m variants, an additional series of experiments was performed using the pure metal-free TK (TK-ΔZn). This choice was based on the stronger interactions observed between the metal-organic knot and the β2m variants. Unlike the metal-containing knots TK-Br and TK-TFA, TK-ΔZn is insoluble in water. Therefore, addition to a protein solution was carried out by first drying an acetonitrile solution of the metal-free knot in a vial and subsequently soaking the

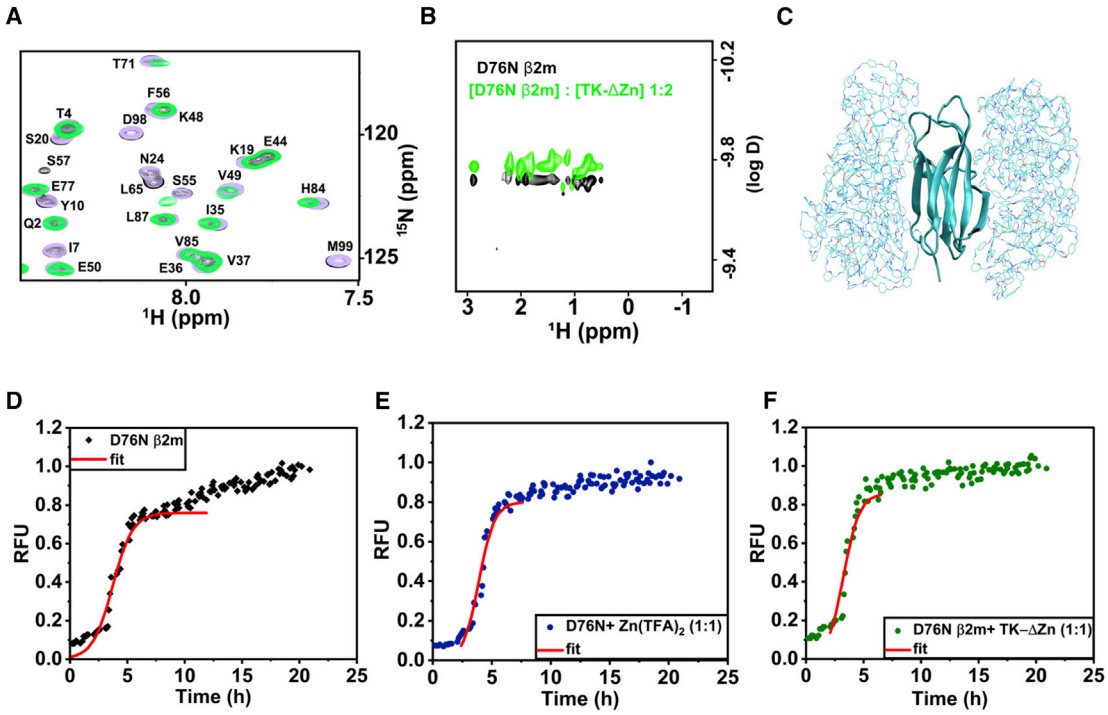

Figure 6. NMR response, MD, and fibrillogenesis assay of D76N β2m in the presence of metal-free TK-ΔZn

(A) Region from the overlay of ^{15}N-^{1}H HSQC spectra of 56 μM D76N β2m without (black contours), with 56 μM TK-ΔZn (pale violet contours), and with 113 μM TK-ΔZn (green contours). The TK-ΔZn concentrations refer to the nominal amount of product dried from CD_3CN and solubilized in the control D76N β2m solution (see text). The full map along with circular dichroism control spectra of the protein alone and in the presence of TK-ΔZn (1:1) are reported in Figure S16.

(B) Overlay of the aliphatic region of DOSY spectra obtained from 56 μM D76N β2m solutions without (black contours) and with 113 μM TK-ΔZn (green contours). The diffusion coefficient of the protein clearly decreases in the presence of the Zn-free knot (see also Figure S17), reflecting an aggregation process that is confirmed by the substantial changes in signal intensity and chemical shifts (A, Figures S15A–S15C and S16A).

(C) Final snapshot after 10-ns MD run showing the protein contacts with TK-ΔZn.

(D–F) ThT fluorescence time course measured for 10 μM D76N β2m solutions kept under fibrillogenic conditions, in the absence (D) and presence of 10 μM Zn-trifluoroacetate (E) and TK-ΔZn (F). Metal-free TK does not prevent fibrillogenesis. ThT assay was also performed with a control solution of protein-containing Zn-trifluoroacetate to rule out any role of the salt in preventing fibrillogenesis. For the reported fitting of D76N β2m fibrillation, t_{half} = 3.72 ± 0.07 h and τ = 0.87 ± 0.06 h (R^2 = 0.965) for the protein alone (D); t_{half} = 3.90 ± 0.06 h and τ = 0.66 ± 0.05 h (R^2 = 0.970) in the presence of $Zn(TFA)_2$ (E); and t_{half} = 3.25 ± 0.08 h and τ = 0.69 ± 0.07 h (R^2 = 0.940) in the presence of TK-ΔZn (F). The steepness of the fibrilllogenesis raising phase in the presence of $Zn(TFA)_2$ and TK-ΔZn is appreciably faster than the value observed with D76N β2m alone.

residue in the same vial with a solution of wild-type or D76N β2m in 95:5 H_2O:D_2O for several minutes. The solution was then transferred to an NMR tube. Dissolution of TK-ΔZn in the aqueous solvent was confirmed by the presence of additional signals in the aromatic region of the ^{1}H NMR spectrum of the sample. To prepare corresponding control samples, the procedure was repeated with vials from which only pure acetonitrile had been evaporated. With both protein variants, the spectral results were similar (Figures 6A, 6B, and S17). An overlay of the ^{15}N-^{1}H HSQC spectra of D76N β2m, without and with TK-ΔZn, is shown in Figure 6A. TK-ΔZn caused changes in the spectrum of the proteins that were significantly different than those caused by the Zn-containing structures. The NH correlation intensities and chemical shifts in the spectra of the proteins were found to be much more perturbed by TK-ΔZn than by the Zn-containing knots. In addition, a complete loss of several cross-peaks was observed, along with generalized and significant shifts of the remaining ones (Figures 6A, S15, and S16). TK-ΔZn did not, however, induce major changes in the secondary structure of the proteins as confirmed by circular dichroism (CD) control (Figure S16B), and the overall chemical shift dispersion was conserved, at

variance with the pattern observed when a perturbation leads to partial or extensive unfolding.[43] When challenged with the three Zn-templated species of different sizes, the signals in the spectrum of the protein showed relatively similar attenuation patterns encompassing characteristic local deviations that were consistent with weak interactions between the proteins and the complexes occurring at preferred surface sites (Figures 2, 3, and S1–S10).

In contrast, TK-ΔZn additions caused substantial protein aggregation, as confirmed by a decrease in the translational diffusion coefficient of the protein measured by DOSY (Figures 6B and S17). The locations exhibiting strong attenuations and loss of signals should define the interface of the protein-TK-ΔZn-protein pairing (Figures S15A–S15C and S16A). No effects on protein signal intensity, chemical shift, or diffusion coefficient were detected in the spectra of control samples, which were prepared with aliquots of pure acetonitrile that had been evaporated in the absence of TK-ΔZn (Figure S17). Consistently with the experimental evidence, MD simulations of wild-type β2m with TK-ΔZn also confirmed a sharp difference with respect to the results obtained with the metal-containing knot. Namely, instead of the variety of transient adducts and no stable complex formation (Figure 4), simulations with the neutral TK-ΔZn species led to aggregation into a single complex involving all solutes and displaying many more protein-knot and knot-knot contacts (Figure 6C) than those transiently sampled in the system wild-type β2m-TK-Br. The protein was observed to be sandwiched between two large aggregates of neutral knots at strands A and G on one side and at strands D, E, and loop AB on the other side (Figure 6C). The simulated contacts were again in good agreement with the corresponding evidence from NMR analysis of the protein/TK-ΔZn systems. The contrasting effects that the metal-containing and metal-free knots had on the protein were consistently confirmed by ThT assay (Figures 6D–6F). Under fibrillogenic conditions, TK-ΔZn did not prevent fibrillogenesis. Neither did zinc trifluoroacetate, which rules out a direct role of the salt, and in particular of Zn^{2+}, in the inhibition of amyloidogenesis.

Administration of TK complexes to a disease model organism

C. elegans is an established model nematode for *in vivo* toxicological studies.[44] Its favorable characteristics include short life cycle, well-known reproductive and lifespan schedule, easy handling and control, and the similarity of its toxicological responses as compared to those of higher organisms. Moreover, transgenic strains of *C. elegans* have proven to be valid animal models for replicating specific features of different pathologies,[45–47] including those related to protein aggregation,[48,49] with a relevance extending also to drug screening.[48,50] The possibility of obtaining *C. elegans* transgenic strains expressing wild-type and highly amyloidogenic variants of β2m[46,51] prompted us to also test the effects of our metal-organic assemblies *in vivo*. Again, those species that exhibited stronger interactions with the proteins *in vitro* (i.e., TK-TFA and TK-Br) were selected for testing *in vivo*. A new strain of the worm CPV27, expressing D76N β2m with a thermo-inducible system,[51] was used, and results with this strain were compared to those observed with *smg-1 (cc546)* ancestral strain (PD8120 strain), which was used as control. Besides exhibiting differences in larval growth and development with respect to the wild type, *C. elegans* models expressing β2m variants are distinctively characterized by behavioral phenotype differences in the survival curve, motility defect, and the brood size.[46,51] The last two factors along with the larval development are used to determine the movement index, i.e., a parameter measured by the INVAPP/Paragon automated system, which has been shown to effectively distinguish *C. elegans* phenotypes.[52] The movement index parameter can be assessed by analysis of

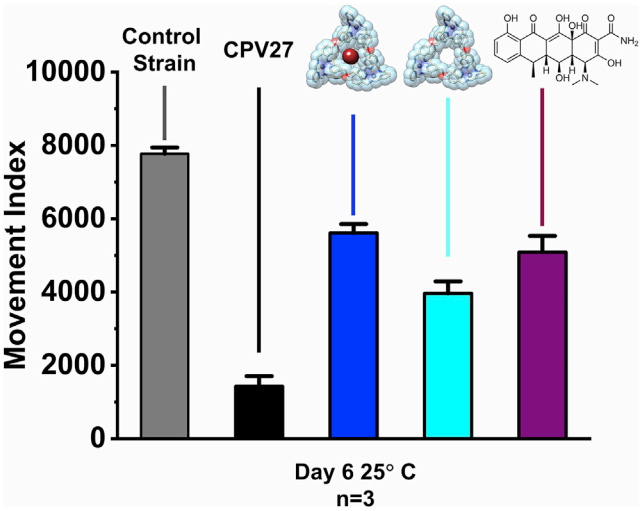

Figure 7. Effect of TK complex administration on *C. elegans* motility

The movement index was measured on worms after 6 days at 25°C. The transgenic nematode strain expressing D76N β2m (CPV27) was treated with the administration of TK-Br (blue), TK-TFA (cyan), or doxycycline (purple), starting at the L4 larval stage. Controls were untreated animals of the same strain (gray) and *smg-1 (cc546)* ancestral strain (black) without any TK complex administration. The movement index values that are reported are means ± standard error of the mean of 3 independent assays. Significance levels of $p < 0.001$, $p < 0.05$, and $p < 0.05$ are obtained for the results with TK-Br, TK-TFA, and doxycycline versus untreated CPV27 worms, according to non-parametric one-way ANOVA.

the developing nematode colonies by automated collection and quantitation of pixel-resolved images.[51,52] The parameter measures the overall nematode culture motility that correlates with the degree of impairment caused by the expression of the amyloidogenic species.[46,51] No fibrillar aggregates have ever been detected in transgenic nematodes expressing the D76N β2m variant,[51] but the observation of oligomeric assemblies of the proteins in the soluble fraction of nematode homogenates correlates with the phenotypic pathology and thus suggests the occurrence of protofibrillar oligomers that are considered responsible for the amyloid damage at the cellular level.[46,51] Figure 7 presents the movement indices, measured after 6 days at 25°C, of several specimens. The measurements were performed on transgenic *C. elegans* populations expressing D76N β2m, without and with the administration of TK-TFA or TK-Br. Administrations began at the last larval stage (L4). The untreated *smg-1 (cc546)* ancestral strain without any TK complex administration was used for the corresponding control measurements. As shown in Figure 7, expression of D76N β2m brought about a significant reduction in motility, and treatment with the metal-templated knots restored that motility. In particular, a substantial recovery in movement index, similar in magnitude to the known doxycycline effect,[51] was observed in the transgenic strain treated with TK-Br, whereas a less pronounced recovery was measured with TK-TFA. Given the inability of the knots to disrupt a preexisting fibrillar assembly (Figure S14A), and assuming that the transgenic phenotype characteristics of *C. elegans* are due to the formation of protofibrillar oligomers,[46,51] one is led to attribute the positive *in vivo* effect of the knots to an efficient inhibition of fibril onset, an effect that is consistent with the evidence from the fibrillogenesis inhibition experiments presented above (Figure 5).

DISCUSSION

Our experimental evidence indicates that dynamic noncovalent interactions between a class of topologically non-trivial metal-organic structures and β2m variants

are responsible for inhibiting fibrillogenesis *in vitro*. The interactions were found to involve primarily sheet I of the β sandwich of the β2m immunoglobulin motif (see Figures 2 and 3), which comprises strands D, E, B, and A (in decreasing order of involvement), and to take place with the Zn complexes [2]C, TK, and BR, but not with the all-organic TK-ΔZn. The effectiveness of the metal-templated species at preventing fibrillogenesis since the early stages of soluble protofibrils was also confirmed *in vivo* in an animal model of amyloid disease. When the metal-organic TK was administered to transgenic *C. elegans* cultures that express D76N β2m, the characteristic phenotypic impairment usually exhibited by the worms was largely reduced and, in some cases, almost completely suppressed, likely because of the inhibition of the early oligomerization steps effected by the knots.

The examined metal-organic structures were found to be capable of establishing dynamic contacts with the surface of the β2m variants in a fast-exchange regime. This type of interaction is comparable to those characteristic of small-molecule chaperones,[16–19] which are able to interfere with the nucleation and fibrillation mechanisms of protein monomers.[53] The molecular chaperone-like properties of the considered metal-organic species are the direct consequence of the structural rigidity imparted by the metal coordination and the chemical affinity contributed by the balanced mix of polar and hydrophobic surface. Due to the unique geometries of the studied metal-based structures, contacts with the surface of the proteins are limited in extent and minimally adaptable, but occur at high frequency, which still allows for sufficient water solvation of the transient adducts that they form with the proteins. In other words, although affecting the hydration of some charged or polar side chains, these interactions allow the protein to remain in solution rather than aggregating and precipitating. The three metal-organic complexes have a similar chemical composition. Also, all three are relatively rigid due to metal coordination. It is their different sizes and their rigidities that largely determine the relative effectiveness of their labile interactions with β2m. In spite of the affinity of the organic scaffolds for β2m, accommodating them on the protein surface to form optimal contacts is apparently progressively hampered with increasing size. Size and rigidity are also determinant to modulate the polar interactions that the metal-templated species may engage by accessing the hydrophilic surface of the protein. Our results show that, of the three tested complexes, the dimensions of the TK match the best compromise between rigidity and affinity. With any of the considered structures, however, these two characteristics preserve the folded structure of the proteins and prevent nucleation and aggregation under fibrillogenic conditions through transient interactions of polar and hydrophobic character that interfere with protein-protein contacts. This is the same class of supramolecular interactions as the repertoire of those established by protein side chains and backbone, namely hydrophobic, polar, and ionic. By engaging these types of interactions that are quite generic for polypeptide chains and certainly not requiring a specific structural complementarity, the considered metal-organic species can compete with the partially misfolded protein assembly leading to fibrils. Fibrillogenesis is in fact the consequence of the stability of a generic intermolecular arrangement that can be attained by any polypeptide chain.[1,3] Therefore, our non-trivial Zn templates should not be selective for β2m. Other proteins with similar chemical characteristics may exhibit an interaction with the tested complexes. This should not be regarded negatively because it does not cancel the property of competing and interfering with fibril assembly.

The surface of TK-ΔZn averaged over 1 ns of MD simulation is similar to that of TK-Br (1,480 $\pm$ 40 and 1,665 $\pm$ 11 Å^2, respectively). However, its greater flexibility determines the effects of its interactions with β2m. When the rigidity of the TK is lost after

Zn^{2+} removal, the hydrophobic forces become predominant and drive the pairing of the metal-free knot to the surface of the protein. This promotes desolvation and aggregation under resting conditions, or partial unfolding, nucleation, and fibrillogenesis under proper perturbation (Figure 6).

We are aware that the present study addresses a single protein system, and concerns may be raised as to how general these findings are. The kind of labile interactions we have demonstrated for β2m and metal-organic knots show detectable preferential affinities, but no particular system specificity, much like the generic character of the interactions leading to polypeptide fibril onset. It is expected, therefore, that similar interaction may also occur with other protein systems, but their generality must be demonstrated by further direct studies.

In conclusion, the prevention of fibrillogenesis by the topologically non-trivial metal-organic structures described in this study appears to be dependent upon the weak polar and hydrophobic contacts that the structures develop with the surface of the target proteins. Contact events consist of frequent labile sampling, which provides a weak and dynamic interaction that supports protein hydration and suppresses aggregation and fibril onset. The weak and dynamic nature of the interaction depends on the rigidity and the dimensions of the metal-templated structures: metal-complex rigidity and size limit the extension of the interaction surface on the protein. Removing the metal from TK leads to a more flexible and hydrophobic structure, the molecule TK-ΔZn, which develops stronger and more extensive contacts with the proteins, thereby promoting hydrophobically driven aggregation.

The use of knots and links as research tools and their investigation as possible drug leads is not unprecedented. The previously mentioned cyclotides[26,27] and knottins[28,29] are peptide-based knots that are being considered with interest for these purposes. Investigation of synthetic non-peptidic molecular knots and links such as those described here is, to our knowledge, novel, and, as suggested by the encouraging results presented above, worthy of further pursuit.

EXPERIMENTAL PROCEDURES

Resource availability

Lead contact

Further information and requests for resources should be directed to and will be fulfilled by the lead contact, G. Esposito (rino.esposito@nyu.edu).

Materials availability

This study did not generate new unique reagents.

Data and code availability

All salient data generated by this study can be found in the article and supplemental information. Additional information is available from the corresponding author upon request.

Materials

Recombinant β2m and D76N β2m were prepared as described previously,[34,41] as were the complexes [2]C, BR, TK-TFA, and TK-Br[30–32] and the cadmium-containing TK (Cd-TK$(TFA)_6$).[54] Cd (II) ions were removed from the TK complex by reduction of the imine bonds to allow for the measurement of interactions between the all-organic knot (TK-ΔZn) and β2m. The organic TK scaffold is easier to obtain by reduction of the Cd-based knots than by reduction of the corresponding Zn-based

complexes. The metal-free TK was obtained as follows: Cd-TK(TFA)$_6$ (25 mg, 9.6 μmol 1 equiv) was added to $NaBH_4$ (29 mg, 384 μmol, 40 equiv) and dry MeOH (10 mL) in a 25-mL reaction flask. The reaction mixture was stirred under Ar atmosphere at room temperature for 15 h. After reaction completion, the mixture was concentrated in a rotary evaporator. To remove unwanted side products (e.g., linear chain fragments) and sodium salts, 10 mL acetonitrile was added, and the reaction mixture was filtered. The crude filtrate containing metal-free TK was further purified by using size-exclusion chromatography with a 90:5:5 mixture of CH_3CN:H_2O:CH_3OH. The purified product was concentrated to dryness under vacuum for 20 h. The NMR and mass spectrometry (MS) characterization data are given: TK-ΔZn: 12.80 mg, 42%; ^{1}H NMR (500 MHz, ACN-d3, 25°C): δ 3.76 (brs, 12H, Ar-CH_2), 4.15 (d, 12H, J = 7.6 Hz, Ar-CH_2), 5.13 (ABq, 12H, J = 11.8 Hz, Ar-CH_2), 6.12 (brs, 6H, Ar-H), 6.39 (d, 12H, J = 8.6 Hz, Ar-H), 6.54 (d, 12H, J = 7.5 Hz, Ar-H), 7.51 (d, 6H, J = 8.6 Hz, Ar-H), 8.06 (t, 3H, J = 6.8 Hz, Ar-H), 8.65 (brs, 6H, Ar-H), 9.53 (brs, 6H, Ar-H); ^{13}C NMR (125 MHz, CD_3CN, 25°C): δ 51.6, 52.9, 68.2, 114.3, 116.6, 118.5, 120.6, 122.5, 129.6, 140.2, 149.0, 149.5, 150.5, 156.3, 157.5; MS (high-resolution electrospray ionization mass spectrometry [ESI-HRMS]): *m/z* Calcd for $(C_{99}H_{94}N_{15}O_6)^{2+}$: 794.3750 $[M+2H]^{2+}$, found: 794.3722 $[M+2H]^{2+}$.

NMR spectroscopy

NMR samples of ^{15}N-uniformly labeled wild-type β2m and D76N β2m were prepared by dissolving lyophilized powders in H_2O/D_2O 95/5 at pH* 5.4–6.1 (wild type) and 6.6–6.8 (D76N) (pH* = uncorrected pHmeter reading) at concentrations in the range of 55–85 μM (wild type) and 50–100 μM (D76N). The Zn-templated species [2]C, TK-TFA, TK-Br, and BR were added by microliter additions from 2 to 2.5 mM aqueous mother solutions, whereas microliter aliquots of 2.5 mM TK-ΔZn dissolved in CD_3CN were dried before being soaked with aqueous protein solution. Some equimolar control samples of TK-Br or BR and wild-type β2m (60 μM) were prepared in ~3–5 mM KBr or NaBr, or 100 mM NaCl. Other control solutions of D76N β2m in 100 mM NaCl, without or with 5 mM $NaHCO_3$ (pH 7.1–7.2), and with [2]C, TK-Br, or BR were also monitored. NMR spectra were collected at 14.0 T, on the Bruker Avance III NMR facility of the Core Technology Platform at New York University Abu Dhabi. The cryoprobe-equipped spectrometer was operated at 600.19 and 60.82 MHz to observe ^{1}H and ^{15}N, respectively. A few spectra were also recorded at 11.7 T (^{1}H and ^{15}N resonance at 500.13 and 50.68 MHz, respectively) on the Bruker Avance machine of the Biophysics laboratory of Udine University. 2D ^{15}N-^{1}H HSQC[36] were recorded over spectral widths of 40 ppm (^{15}N, t_1) and 15 ppm (^{1}H, t_2) and digitized over 128–192 and 2,048 points, respectively. For each t_1 dimension point, 16, 32, or 64 scans were accumulated and quadrature was accomplished by gradient-assisted coherence selection (echo-antiecho).[55]. DOSY[38] spectra for the determination of diffusion coefficients were acquired by 2D ^{1}H DSTEBPP (double stimulated echo bipolar pulse) experiments.[56] The z axis gradient strength was varied linearly from 10% to 90% of its maximum value (~60 G/cm), and matrices of 2,048 by 40–80 points were collected by accumulating 32–64 scans per gradient increment. Water suppression was achieved in DOSY experiments by appending to the DSTEBPP sequence a pair of WATERGATE[57] elements, according to the excitation-sculpting[58] mode, or, in the HSQC experiments,[59] using a flip-back pulse. All of the measurements were performed at 25°C.

MD simulations

The molecular structures of β2m and D76N β2m were based on the available crystallographic coordinates with PDB codes 3HLA[40] and 4FXL4, respectively. The protonation states of titratable residues were assigned using the Bluues server available at https://protein.bio.unipd.it/bluues/.[60,61] Protons were added using the

pdb2gmx utility of the GROMACS simulation package,[62] and topology and coordinate files were generated using the psfgen utility of the NAMD simulation software.[63] The modeled [2]C, TK, and BR species were built using the reference coordinate set.[30–32] TK-Br was obtained from the reference coordinates by removing the Zn and TFA ions of the central $[ZnBr(TFA)_3]^{2-}$ complexes.[31] TK-ΔZn was obtained by replacement of the three axial TFAs of the reference structure with water, removal of the $[ZnBr(TFA)_3]^{2-}$ complexes and the coordinating Zn ions with the accompanying waters, and reduction of the exocyclic imine nitrogens. The Amber99sb-ildn forcefield[64] was used for all of the simulations. The temperature was kept constant at 310 K using Langevin dynamics with a relaxation time of 1 ps. β2m variants were restrained, with residues C25 and C80 at the center of a cube where 26 knot molecules were regularly arranged with a spacing of 36 Å. All of the species were restrained within a sphere with a radius of 60 Å centered on the protein through a harmonic potential active beyond the radius. After 1,000 minimization steps, the system was heated at 310 K in 100 ps and, after additional 1-ns simulation, a 10-ns MD simulation was performed. Contacts were defined when the distance between two heavy atoms was less than the sum of their van der Waals radii plus 1 Å.[65] Zn and Br bond distances were taken from published structures,[30–32] whereas the corresponding bond and bond angle and torsion angle force constants were set to 400 kcal/(Å^2 mol), 50 kcal/(Å^2 mol), and 0.0, respectively. The nonbonded parameters for the same atoms were taken from the Amber forcefield. Charges were assigned using the Gasteiger and Marsili method for organic molecules[66,67] and locally modified for the presence of Zn and Br. MD simulations were performed with the program NAMD 2.9[63] using the generalized Born surface area (GBSA) implicit solvent model.[68] GB radii were computed according to the Onufriev-Bashford-Case (OBC) model,[69] and salt effects were implemented in NAMD GB models through a screening function.[70] Surface areas were calculated from the area sampled by a sphere of 1.4 Å radius, as averaged over 26 copies of the considered species submitted to 1 ns of MD.

Fibrillogenesis and ThT fluorescence assay

A solution of D76N β2m (2 mg mL^{-1}) in water (pH 6.6) was centrifuged, passed through a 0.22-μm filter, and diluted to 20 μM either with water or a solution of [2]C, TK-TFA, TK-Br, BR, or TK-ΔZn until the protein and knot/link were at equimolar concentrations. The solutions were incubated at 37°C and vigorously stirred. Aliquots were taken at different times and submitted to ThT fluorescence analysis. The procedure was performed in triplicate for each sample.

ThT fluorescence assays (445 nm/480 nm excitation/emission)[71] on fibrillogenesis aliquots were conducted at 37°C on a PerkinElmer EnSpire 2300 fluorimeter in the presence of 10 μM ThT in 50 mM glycine buffer, pH 8.3.

ThT fluorescence time courses were also measured for 10 μM D76N β2m solutions kept under fibrillogenic conditions (orbital shaking at 700 rpm at 37°C for 36 h with 40 μM ThT, pH 7.1). The fluorescence was monitored every 10 min, after stopping the shaking, by means of a plate-reading fluorimeter. The plotted values are the averages over the readings from three different wells. The fibrillogenesis kinetics represented by the ThT fluorescence raising phase were fitted by a Boltzmann sigmoidal function plotted in red in Figures 6D and 6E and described by the following equation:

$$y = \frac{\alpha}{\left(1 + exp\left(-\frac{(t - t_{half})}{\tau}\right)\right)}$$

where y is the ThT fluorescence intensity, a is the difference between initial and final fluorescence intensity values of the raising phase, t_{half} represents the time at half-height of that fluorescence excursion, t is the time, and τ is the time constant describing the steepness of the curve.

C. elegans experiments

Ancestral *smg1* (*cc*546) strain was purchased from the Caenorhabditis Genetics Center (University of Minnesota, St. Paul, MN). Construction and characteristics of the transgenic *C. elegans* strain expressing D76N β2 m (CPV27) have been previously described.[51] Nematode offspring of CPV27 and ancestral strains were maintained and propagated at 16°C on solid Nematode Growth Medium (NGM) supplemented with OP50 *Escherichia coli* preparations (Caenorhabditis Genetics Center) for feeding. To obtain age-synchronized animals, adult nematodes were bleached with alkaline solution (500 mM NaOH, 1.5% NaClO) and the isolated eggs were maintained at 16°C. When the L1 larval stage was reached, the expression of D76N β2m was induced by shifting the temperature to 25°C to trigger the transgene expression system.[51] Three synchronized nematodes at the L4 larval stage were placed into NGM agar plates and seeded with tetracycline-resistant *E. coli* (HT115) in the presence (100 μM) or absence of doxycycline or TK-Br or TK-TFA in distilled or EPA water. Plates were imaged 6 days later using the recently developed INVAPP/Paragon system and motility was scored as previously described.[52] Controls were grown with distilled water only, with either the transgenic or the *smg-1 (cc*546*)* ancestral strain. Three independent assays were performed for each treatment or non-treatment.

AFM analysis

Samples for AFM were prepared by drop-casting on silicon wafer 10 μL aliquots of the solutions, which had undergone 36 h of fibrillogenic treatment on silicon wafer. The silicon substrates were 10 × 10 mm in size. Before and after drying for 2 days under ambient conditions, these square-shaped substrates were mounted on an AFM substrate holder. The surface topography of all of these samples, under wet conditions or after 2 days of drying (before and after drying), were analyzed by AFM (Model 5500 Atomic Force Microscope, Keysight Technologies, Santa Rosa, CA) in non-contact mode. We used Si cantilevers (Nanosensors, Neuchatel, Switzerland) with a resonant frequency of 200–500 kHz and a force constant of 10–130 Nm^{-1} to acquire height, phase, and amplitude imaging simultaneously. The set point values were typically maintained at 2.25 V. Gwyddion free software (version 2.47) was used for post-processing the acquired topographic scans.

SUPPLEMENTAL INFORMATION

Supplemental information can be found online at https://doi.org/10.1016/j.xcrp.2021.100477.

ACKNOWLEDGMENTS

This work received financial support from New York University Abu Dhabi, the Research Enhancement Fund (REF) at NYUAD, and the Abu Dhabi Emirate Department of Education and Knowledge (ADEK), project no. AARE 18-115. We acknowledge New York University Abu Dhabi for the access to the Core Technology Platform. We also thank Cyril Aubry for some AFM experiments and Makek Ads for the assistance.

AUTHOR CONTRIBUTIONS

Conceptualization, T.P., Y.H., C.C., A.T., and G.E.; methodology, T.P., A.T., V.B., F.F., and G.E.; investigation, T.P., Y.H., C.C., A.T., G.E., S.G., G.F., V.M., S.K.S.,

R.J., G.P., and F.F.; writing – original draft, J.-C.O., A.T., and G.E.; writing – review & editing, all authors; funding acquisition, A.T. and G.E.; resources, T.P., S.G., G.F., and V.M.; supervision, A.T. and G.E.

DECLARATION OF INTERESTS

The authors declare no competing interests.

Received: November 3, 2020
Revised: May 24, 2021
Accepted: June 4, 2021
Published: June 25, 2021

REFERENCES

1. Knowles, T.P.J., Vendruscolo, M., and Dobson, C.M. (2014). The amyloid state and its association with protein misfolding diseases. Nat. Rev. Mol. Cell Biol. *15*, 384–396.

2. Pieters, B.J.G.E., van Eldijk, M.B., Nolte, R.J.M., and Mecinović, J. (2016). Natural supramolecular protein assemblies. Chem. Soc. Rev. *45*, 24–39.

3. Chiti, F., and Dobson, C.M. (2006). Protein misfolding, functional amyloid, and human disease. Annu. Rev. Biochem. *75*, 333–366.

4. Cheng, B., Gong, H., Xiao, H., Petersen, R.B., Zheng, L., and Huang, K. (2013). Inhibiting toxic aggregation of amyloidogenic proteins: a therapeutic strategy for protein misfolding diseases. Biochim. Biophys. Acta *1830*, 4860–4871.

5. Ramazzotti, M., Melani, F., Marchi, L., Mulinacci, N., Gestri, S., Tiribilli, B., and Degl'Innocenti, D. (2016). Mechanisms for the inhibition of amyloid aggregation by small ligands. Biosci. Rep. *36*, 1–13.

6. Bulawa, C.E., Connelly, S., Devit, M., Wang, L., Weigel, C., Fleming, J.A., Packman, J., Powers, E.T., Wiseman, R.L., Foss, T.R., et al. (2012). Tafamidis, a potent and selective transthyretin kinetic stabilizer that inhibits the amyloid cascade. Proc. Natl. Acad. Sci. USA *109*, 9629–9634.

7. Kayed, R., Head, E., Thompson, J.L., McIntire, T.M., Milton, S.C., Cotman, C.W., and Glabe, C.G. (2003). Common structure of soluble amyloid oligomers implies common mechanism of pathogenesis. Science *300*, 486–489.

8. Siemers, E.R., Friedrich, S., Dean, R.A., Gonzales, C.R., Farlow, M.R., Paul, S.M., and Demattos, R.B. (2010). Safety and changes in plasma and cerebrospinal fluid amyloid beta after a single administration of an amyloid beta monoclonal antibody in subjects with Alzheimer disease. Clin. Neuropharmacol. *33*, 67–73.

9. La Porte, S.L., Bollini, S.S., Lanz, T.A., Abdiche, Y.N., Rusnak, A.S., Ho, W.H., Kobayashi, D., Harrabi, O., Pappas, D., Mina, E.W., et al. (2012). Structural basis of C-terminal β-amyloid peptide binding by the antibody ponezumab for the treatment of Alzheimer's disease. J. Mol. Biol. *421*, 525–536.

10. Dumoulin, M., Last, A.M., Desmyter, A., Decanniere, K., Canet, D., Larsson, G., Spencer, A., Archer, D.B., Sasse, J., Muyldermans, S., et al. (2003). A camelid antibody fragment inhibits the formation of amyloid fibrils by human lysozyme. Nature *424*, 783–788.

11. Raimondi, S., Porcari, R., Mangione, P.P., Verona, G., Marcoux, J., Giorgetti, S., Taylor, G.W., Ellmerich, S., Ballico, M., Zanini, S., et al. (2017). A specific nanobody prevents amyloidogenesis of D76N β_2-microglobulin in vitro and modifies its tissue distribution in vivo. Sci. Rep. *7*, 46711.

12. Marcoux, J., Mangione, P.P., Porcari, R., Degiacomi, M.T., Verona, G., Taylor, G.W., Giorgetti, S., Raimondi, S., Sanglier-Cianférani, S., Benesch, J.L., et al. (2015). A novel mechano-enzymatic cleavage mechanism underlies transthyretin amyloidogenesis. EMBO Mol. Med. *7*, 1337–1349.

13. Carver, J.A., Rekas, A., Thorn, D.C., and Wilson, M.R. (2003). Small heat-shock proteins and clusterin: intra- and extracellular molecular chaperones with a common mechanism of action and function? IUBMB Life *55*, 661–668.

14. Raman, B., Ban, T., Sakai, M., Pasta, S.Y., Ramakrishna, T., Naiki, H., Goto, Y., and Rao, ChM. (2005). AlphaB-crystallin, a small heat-shock protein, prevents the amyloid fibril growth of an amyloid β-peptide and β2-microglobulin. Biochem. J. *392*, 573–581.

15. Esposito, G., Garvey, M., Alverdi, V., Pettirossi, F., Corazza, A., Fogolari, F., Polano, M., Mangione, P.P., Giorgetti, S., Stoppini, M., et al. (2013). Monitoring the interaction between β2-microglobulin and the molecular chaperone αB-crystallin by NMR and mass spectrometry: αB-crystallin dissociates β2-microglobulin oligomers. J. Biol. Chem. *288*, 17844–17858.

16. Powers, E.T., Morimoto, R.I., Dillin, A., Kelly, J.W., and Balch, W.E. (2009). Biological and chemical approaches to diseases of proteostasis deficiency. Annu. Rev. Biochem. *78*, 959–991.

17. Giorgetti, S., Raimondi, S., Pagano, K., Relini, A., Bucciantini, M., Corazza, A., Fogolari, F., Codutti, L., Salmona, M., Mangione, P., et al. (2011). Effect of tetracyclines on the dynamics of formation and destructuration of beta2-microglobulin amyloid fibrils. J. Biol. Chem. *286*, 2121–2131.

18. Wang, Y.-J., Di, X.-J., and Mu, T.-W. (2014). Using pharmacological chaperones to restore proteostasis. Pharmacol. Res. *83*, 3–9.

19. Convertino, M., Das, J., and Dokholyan, N.V. (2016). Pharmacological Chaperones: Design and Development of New Therapeutic Strategies for the Treatment of Conformational Diseases. ACS Chem. Biol. *11*, 1471–1489.

20. Montagna, G., Cazzulani, B., Obici, L., Uggetti, C., Giorgetti, S., Porcari, R., Ruggiero, R., Mangione, P.P., Brambilla, M., Lucchetti, J., et al. (2013). Benefit of doxycycline treatment on articular disability caused by dialysis related amyloidosis. Amyloid *20*, 173–178.

21. Stoilova, T., Colombo, L., Forloni, G., Tagliavini, F., and Salmona, M. (2013). A new face for old antibiotics: tetracyclines in treatment of amyloidoses. J. Med. Chem. *56*, 5987–6006.

22. Hsieh, S., Chang, C.W., and Chou, H.H. (2013). Gold nanoparticles as amyloid-like fibrillogenesis inhibitors. Colloids Surf. B Biointerfaces *112*, 525–529.

23. Moore, K.A., Pate, K.M., Soto-Ortega, D.D., Lohse, S., van der Munnik, N., Lim, M., Jackson, K.S., Lyles, V.D., Jones, L., Glassgow, N., et al. (2017). Influence of gold nanoparticle surface chemistry and diameter upon Alzheimer's disease amyloid-β protein aggregation. J. Biol. Eng. *11*, 5.

24. Cantarutti, C., Raimondi, S., Brancolini, G., Corazza, A., Giorgetti, S., Ballico, M., Zanini, S., Palmisano, G., Bertoncin, P., Marchese, L., et al. (2017). Citrate-stabilized gold nanoparticles hinder fibrillogenesis of a pathological variant of β_2-microglobulin. Nanoscale *9*, 3941–3951.

25. Cabaleiro-Lago, C., Szczepankiewicz, O., and Linse, S. (2012). The effect of nanoparticles on amyloid aggregation depends on the protein stability and intrinsic aggregation rate. Langmuir *28*, 1852–1857.

26. Craik, D.J., and Du, J. (2017). Cyclotides as drug design scaffolds. Curr. Opin. Chem. Biol. *38*, 8–16.

27. Huang, Y.-H., Du, Q., and Craik, D.J. (2019). Cyclotides: disulfide-rich peptide toxins in plants. Toxicon *172*, 33–44.

28. Moore, S.J., and Cochran, J.R. (2012). Engineering knottins as novel binding agents. Methods Enzymol. *503*, 223–251.

29. Avrutina, O. (2016). Synthetic Cystine-Knot Miniproteins - Valuable Scaffolds for Polypeptide Engineering. Adv. Exp. Med. Biol. *917*, 121–144.

30. Prakasam, T., Lusi, M., Elhabiri, M., Platas-Iglesias, C., Olsen, J.-C., Asfari, Z., Cianférani-Sanglier, S., Debaene, F., Charbonnière, L.J., and Trabolsi, A. (2013). Simultaneous self-assembly of a [2]catenane, a trefoil knot, and a Solomon link from a simple pair of ligands. Angew. Chem. Int. Ed. Engl. *52*, 9956–9960.

31. Bilbeisi, R.A., Prakasam, T., Lusi, M., El Khoury, R., Platas-Iglesias, C., Charbonnière, L.J., Olsen, J.C., Elhabiri, M., and Trabolsi, A. (2016). [C-H···anion] interactions mediate the templation and anion binding properties of topologically non-trivial metal-organic structures in aqueous solutions. Chem. Sci. (Camb.) *7*, 2524–2531.

32. Chichak, K.S., Cantrill, S.J., Pease, A.R., Chiu, S.-H., Cave, G.W.V., Atwood, J.L., and Stoddart, J.F. (2004). Molecular borromean rings. Science *304*, 1308–1312.

33. Gejyo, F., Yamada, T., Odani, S., Nakagawa, Y., Arakawa, M., Kunitomo, T., Kataoka, H., Suzuki, M., Hirasawa, Y., Shirahama, T., et al. (1985). A new form of amyloid protein associated with chronic hemodialysis was identified as β 2-microglobulin. Biochem. Biophys. Res. Commun. *129*, 701–706.

34. Valleix, S., Gillmore, J.D., Bridoux, F., Mangione, P.P., Dogan, A., Nedelec, B., Boimard, M., Touchard, G., Goujon, J.M., Lacombe, C., et al. (2012). Hereditary systemic amyloidosis due to Asp76Asn variant β2-microglobulin. N. Engl. J. Med. *366*, 2276–2283.

35. Mangione, P.P., Esposito, G., Relini, A., Raimondi, S., Porcari, R., Giorgetti, S., Corazza, A., Fogolari, F., Penco, A., Goto, Y., et al. (2013). Structure, folding dynamics, and amyloidogenesis of D76N β2-microglobulin: roles of shear flow, hydrophobic surfaces, and α-crystallin. J. Biol. Chem. *288*, 30917–30930.

36. Bodenhausen, G., and Ruben, D.J. (1980). Natural abundance nitrogen-15 NMR by enhanced heteronuclear spectroscopy. Chem. Phys. Lett. *69*, 185–189.

37. Mulder, F.A., Schipper, D., Bott, R., and Boelens, R. (1999). Altered flexibility in the substrate-binding site of related native and engineered high-alkaline Bacillus subtilisins. J. Mol. Biol. *292*, 111–123.

38. Morris, K.F., and Johnson, C.S. (1992). Diffusion-ordered two-dimensional nuclear magnetic resonance spectroscopy. J. Am. Chem. Soc. *114*, 3139–3141.

39. Verdone, G., Corazza, A., Viglino, P., Pettirossi, F., Giorgetti, S., Mangione, P., Andreola, A., Stoppini, M., Bellotti, V., and Esposito, G. (2002). The solution structure of human β2-microglobulin reveals the prodromes of its amyloid transition. Protein Sci. *11*, 487–499.

40. Bjorkman, P.J., Saper, M.A., Samraoui, B., Bennett, W.S., Strominger, J.L., and Wiley, D.C. (1987). Structure of the human class I histocompatibility antigen, HLA-A2. Nature *329*, 506–512.

41. Esposito, G., Michelutti, R., Verdone, G., Viglino, P., Hernández, H., Robinson, C.V., Amoresano, A., Dal Piaz, F., Monti, M., Pucci, P., et al. (2000). Removal of the N-terminal hexapeptide from human β2-microglobulin facilitates protein aggregation and fibril formation. Protein Sci. *9*, 831–845.

42. Geddes, C.D., Apperson, K., Karolin, J., and Birch, D.J. (2001). Chloride-sensitive fluorescent indicators. Anal. Biochem. *293*, 60–66.

43. Rennella, E., Corazza, A., Giorgetti, S., Fogolari, F., Viglino, P., Porcari, R., Verga, L., Stoppini, M., Bellotti, V., and Esposito, G. (2010). Folding and fibrillogenesis: clues from β2-microglobulin. J. Mol. Biol. *401*, 286–297.

44. Boyd, W.A., Smith, M.V., and Freedman, J.H. (2012). *Caenorhabditis elegans* as a model in developmental toxicology. Methods Mol. Biol. *889*, 15–24.

45. Forsythe, M.E., Love, D.C., Lazarus, B.D., Kim, E.J., Prinz, W.A., Ashwell, G., Krause, M.W., and Hanover, J.A. (2006). *Caenorhabditis elegans* ortholog of a diabetes susceptibility locus: oga-1 (O-GlcNAcase) knockout impacts O-GlcNAc cycling, metabolism, and dauer. Proc. Natl. Acad. Sci. USA *103*, 11952–11957.

46. Diomede, L., Soria, C., Romeo, M., Giorgetti, S., Marchese, L., Mangione, P.P., Porcari, R., Zorzoli, I., Salmona, M., Bellotti, V., and Stoppini, M. (2012). C. elegans expressing human β2-microglobulin: a novel model for studying the relationship between the molecular assembly and the toxic phenotype. PLoS ONE *7*, e52314.

47. Li, J., and Le, W. (2013). Modeling neurodegenerative diseases in *Caenorhabditis elegans*. Exp. Neurol. *250*, 94–103.

48. McColl, G., Roberts, B.R., Pukala, T.L., Kenche, V.B., Roberts, C.M., Link, C.D., Ryan, T.M., Masters, C.L., Barnham, K.J., Bush, A.I., and Cherny, R.A. (2012). Utility of an improved model of amyloid-beta (A β_{1-42}) toxicity in Caenorhabditis elegans for drug screening for Alzheimer's disease. Mol. Neurodegener. *7*, 57.

49. Madhivanan, K., Greiner, E.R., Alves-Ferreira, M., Soriano-Castell, D., Rouzbeh, N., Aguirre, C.A., Paulsson, J.F., Chapman, J., Jiang, X., Ooi, F.K., et al. (2018). Cellular clearance of circulating transthyretin decreases cell-nonautonomous proteotoxicity in *Caenorhabditis elegans*. Proc. Natl. Acad. Sci. USA *115*, E7710–E7719.

50. Alavez, S., Vantipalli, M.C., Zucker, D.J., Klang, I.M., and Lithgow, G.J. (2011). Amyloid-binding compounds maintain protein homeostasis during ageing and extend lifespan. Nature *472*, 226–229.

51. Faravelli, G., Raimondi, S., Marchese, L., Partridge, F.A., Soria, C., Mangione, P.P., Canetti, D., Perni, M., Aprile, F.A., Zorzoli, I., et al. (2019). C. elegans expressing D76N β_2-microglobulin: a model for in vivo screening of drug candidates targeting amyloidosis. Sci. Rep. *9*, 19960.

52. Partridge, F.A., Brown, A.E., Buckingham, S.D., Willis, N.J., Wynne, G.M., Forman, R., Else, K.J., Morrison, A.A., Matthews, J.B., Russell, A.J., et al. (2018). An automated high-throughput system for phenotypic screening of chemical libraries on C. elegans and parasitic nematodes. Int. J. Parasitol. Drugs Drug Resist. *8*, 8–21.

53. Naiki, H., Hashimoto, N., Suzuki, S., Kimura, H., Nakakuki, K., and Gejyo, F. (1997). Establishment of a kinetic model of dialysis-related amyloid fibril extension in vitro. Amyloid *4*, 223–232.

54. Prakasam, T., Bilbeisi, R.A., Lusi, M., Olsen, J.-C., Platas-Iglesias, C., and Trabolsi, A. (2016). Post-synthetic modifications of cadmium-based knots and links. Chem. Commun. (Camb.) *52*, 7398–7401.

55. Keeler, J., Clowes, R.T., Davis, A.L., and Laue, E.D. (1994). Pulsed-field gradients: theory and practice. Methods Enzymol. *239*, 145–207.

56. Jerschow, A., and Müller, N. (1998). Convection Compensation in Gradient Enhanced Nuclear Magnetic Resonance Spectroscopy. J. Magn. Reson. *132*, 13–18.

57. Piotto, M., Saudek, V., and Sklenár, V. (1992). Gradient-tailored excitation for single-quantum NMR spectroscopy of aqueous solutions. J. Biomol. NMR *2*, 661–665.

58. Hwang, T.L., and Shaka, A.J. (1995). Water Suppression That Works. Excitation Sculpting Using Arbitrary Wave-Forms and Pulsed-Field Gradients. J. Magn. Reson. A *112*, 275–279.

59. Grzesiek, S., and Bax, A. (1993). The importance of not saturating water in protein NMR. Application to sensitivity enhancement and NOE measurements. J. Am. Chem. Soc. *115*, 12593–12594.

60. Fogolari, F., Corazza, A., Yarra, V., Jalaru, A., Viglino, P., and Esposito, G. (2012). Bluues: a program for the analysis of the electrostatic properties of proteins based on generalized Born radii. BMC Bioinformatics *13* (*Suppl 4*), S18.

61. Walsh, I., Minervini, G., Corazza, A., Esposito, G., Tosatto, S.C., and Fogolari, F. (2012). Bluues server: electrostatic properties of wild-type and mutated protein structures. Bioinformatics *28*, 2189–2190.

62. Berendsen, H.J.C., van der Spoel, D., and van Drunen, R. (1995). GROMACS: a message-passing parallel molecular dynamics implementation. Comput. Phys. Commun. *91*, 43–56.

63. Kalé, L., Skeel, R., Bhandarkar, M., Brunner, R., Gursoy, A., Krawetz, N., Phillips, J., Shinozaki, A., Varadarajan, K., and Schulten, K. (1999). NAMD2: Greater Scalability for Parallel Molecular Dynamics. J. Comput. Phys. *151*, 283–312.

64. Lindorff-Larsen, K., Piana, S., Palmo, K., Maragakis, P., Klepeis, J.L., Dror, R.O., and Shaw, D.E. (2010). Improved side-chain torsion potentials for the Amber ff99SB protein force field. Proteins *78*, 1950–1958.

65. Berrera, M., Molinari, H., and Fogolari, F. (2003). Amino acid empirical contact energy definitions for fold recognition in the space of contact maps. BMC Bioinformatics *4*, 8.

66. Gasteiger, J., and Marsili, M. (1978). A new model for calculating atomic charges in molecules. Tetrahedron Lett. *19*, 3181–3184.

67. Gasteiger, J., and Marsili, M.I. (1980). Iterative partial equalization of orbital electronegativity—a rapid access to atomic charges. Tetrahedron *36*, 3219–3228.

68. Bashford, D., and Case, D.A. (2000). Generalized born models of macromolecular solvation effects. Annu. Rev. Phys. Chem. *51*, 129–152.

69. Onufriev, A., Bashford, D., and Case, D.A. (2004). Exploring protein native states and large-scale conformational changes with a modified generalized born model. Proteins *55*, 383–394.

70. Srinivasan, J., Trevathan, M.W., Beroza, P., and Case, D.A. (1999). Application of a pairwise generalized Born model to proteins and nucleic acids: inclusion of salt effects. Theor. Chem. Acc. *101*, 426–434.

71. Gade Malmos, K., Blancas-Mejia, L.M., Weber, B., Buchner, J., Ramirez-Alvarado, M., Naiki, H., and Otzen, D. (2017). ThT 101: a primer on the use of thioflavin T to investigate amyloid formation. Amyloid *24*, 1–16.